

Symmetry Classification for Alternating Excitons in Two-Dimensional Altermagnets

Jiayu David Cao, Konstantin S. Denisov, Yuntian Liu,* and Igor Žutić

Department of Physics, University at Buffalo, State University of New York, Buffalo, New York 14260, USA

Excitons, bound electron-holes states, often dominate the optical response of two-dimensional (2D) materials and reflect their inherent properties, including spin-orbit coupling, magnetic ordering, or band topology. By focusing on a growing class of collinear antiferromagnets with a nonrelativistic spin splitting, referred to also as altermagnets (AM), we propose a theoretical framework based on the spin space group (SSG) to elucidate their resulting excitons. Our approach is illustrated on 2D AM with spin-polarized valleys, where we classify the combination of conduction and valence bands by the SSG representations into two cases that hosts bright s -like and p -like excitons, respectively. This analysis is further supported by effective Hamiltonians and the Bethe–Salpeter equation. We identify the excitonic optical selection rules from the calculated absorption spectra and the symmetry of bright excitons from their momentum space envelope functions. Our framework provides optical fingerprints for various cases of AM, while their tunability, such as the strain-induced valley splitting, is also transferred to excitons allowing, additionally, valley-polarized photocurrent generation.

A growing class of two-dimensional (2D) materials is characterized by reduced dielectric screening which enhances Coulomb interactions and many-body effects [1–9]. The resulting excitons, as exemplified in 2D transition metal dichalcogenides (TMDs) [10], can propagate over macroscopic distance [11, 12], have orders of magnitude larger binding energy than their bulk counterparts [13] and chiral optical selection rules influenced by the band spin splitting from strong spin-orbit coupling (SOC) [14–18]. K and K' valleys, connected through time-reversal symmetry, are coupled to light with positive and negative helicity (σ^+ , σ^-), where the SOC leads to the spin-valley locking. Excitons in TMDs provide a sensitive probe for proximity effects, from modified SOC and magnetism to charge-density wave and changing topology [19–24].

With a huge interest in altermagnets (AM) [25–32], sharing vanishing magnetization with TMDs, but having broken time-reversal symmetry and spin splitting unrelated to SOC [33–36], it would be important to elucidate the character of their excitons. Unlike many other magnetic, AM offer a remarkable tunability of the spin splitting with alternating sign across the Brillouin zone [37, 38]. Several questions then naturally arise: (i) What are the underlying optical selection rules for excitons in AM? (ii) What is the implication of the versatile tunability of AM on their excitons and optical response? (iii) Could the excitonic properties offer an alternative signature of AM and complement the prior studies?

Building on the recent progress in 2DAM candidates [39–43], here we address these questions using a framework of the spin space group (SSG) [44–51], particularly suitable to study AM as well as a broader class of unconventional magnets [52–56]. We focus on the d -wave 2DAM, shown in Fig. 1(a), that host spin-polarized X and Y valleys. Unlike the K and K' valleys in TMDs, X and Y valleys are connected by the SSG symmetry operation $\{T||C_{4z}\}$, which combines time-reversal symmetry

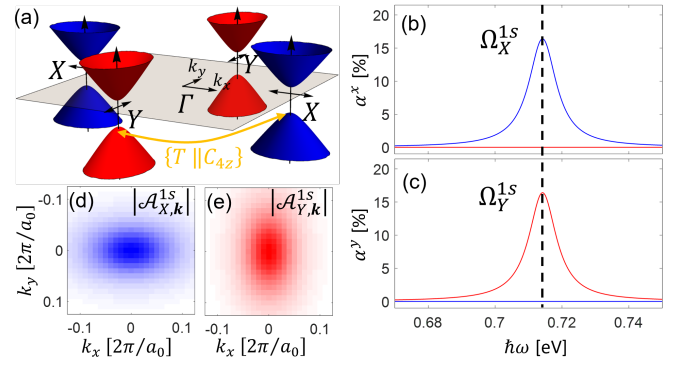


FIG. 1. (a) Schematic illustrations of the band structure of a d -wave 2DAM with spin-polarized X (blue) and Y (red) valleys, connected by the symmetry operation $\{T||C_{4z}\}$. (b), (c) Absorption spectra of x and y polarized light, with $\Omega_{X,Y}^{1s}$ the excitonic energies in the valleys X/Y, for the case 1 (see text). (d), (e) The corresponding wave functions in the momentum space of $1s$ -like excitons in the X and Y valleys, with a_0 for the lattice constant.

and real-space 90° rotation along the z axis [Fig. 1]. Complementing SSG with the symmetry analysis of effective Hamiltonians and Bethe-Salpeter equation (BSE), we establish the excitonic optical selection rules for 2DAM, revealing alternating exciton wave function and x/y linearly polarized light, that provide striking signatures for these magnets. According to the SSG representations of the conduction and valence bands in the X and Y valleys, 2DAM can be classified into two cases (C1, C2), that separately hosts bright s -like and p -like excitons.

An exciton formed with electrons and holes from the valley τ is expressed as $|\tau, S\rangle = \sum_{\mathbf{k}} \mathcal{A}_{\tau,\mathbf{k}}^S \hat{c}_{\tau,\mathbf{k}}^\dagger \hat{c}_{\tau,\mathbf{k}} |GS\rangle$, where S labels the excitonic state, \mathbf{k} is the wave vector measured from $\tau = X, Y$, $\mathcal{A}_{\tau,\mathbf{k}}^S$ is the \mathbf{k} -space exciton envelope wave function, $\hat{c}_{\tau,\mathbf{k}}^\dagger$ ($\hat{c}_{\tau,\mathbf{k}}$) is the creation (annihilation) operator of the electron and $|GS\rangle$ is the ground state with fully occupied valence (v) and empty conduction (c) bands. The strength of an optical transition with

* yliu369@buffalo.edu

polarization σ to an exciton $|\tau, S\rangle$ is given by $M_{\tau,\sigma}^S$ as

$$\mathcal{M}_{\tau,\sigma}^S = \frac{1}{A} \sum_{\mathbf{k}} \mathcal{D}_{\tau,\mathbf{k}}^\sigma [\mathcal{A}_{\tau,\mathbf{k}}^S]^*, \quad (1)$$

where A is the 2D unit area, $\mathcal{D}_{\tau,\mathbf{k}}^\sigma = \langle \tau, c\mathbf{k} | \hat{v}_\sigma | \tau, v\mathbf{k} \rangle$, is the the velocity matrix element, with $|\tau, c(v)\mathbf{k}\rangle$ for an electron (hole) state $\mathcal{A}_{\tau,\mathbf{k}}^S$ and the corresponding exciton energy Ω_τ^S are obtained by solving the BSE $\sum_{\mathbf{k}'} H_{\text{BSE}}(\mathbf{k}, \mathbf{k}') \mathcal{A}_{\tau,\mathbf{k}'}^S = \Omega_\tau^S \mathcal{A}_{\tau,\mathbf{k}}^S$, with the BSE Hamiltonian [57–61] defined as

$$H_{\text{BSE}}(\mathbf{k}, \mathbf{k}') = E_{cv}(\mathbf{k}) - \frac{1}{A} \sum_{\mathbf{k}'} V(|\mathbf{k}-\mathbf{k}'|) \langle c\mathbf{k} | c\mathbf{k}' \rangle \langle v\mathbf{k}' | v\mathbf{k} \rangle \quad (2)$$

where $E_{cv}(\mathbf{k}) = \epsilon_c(\mathbf{k}) - \epsilon_v(\mathbf{k})$ is the \mathbf{k} -dependent energy difference between conduction and valence bands, the valley index is included in the band index $c(v)$, and $V(|\mathbf{q}|)$ is the Fourier component of the screened Coulomb interaction [62, 63]. While $\mathcal{A}_{\tau,\mathbf{k}}^S$ can be obtained by numerically solving the BSE, some important properties of excitons can be obtained by the following symmetry analysis.

In the 2D isotropic limit, H_{BSE} commutes with symmetry operation $C_{\infty z}$ around the z axis, recovering a 2D hydrogen model where excitonic states are labeled by the principal and orbital angular momentum number ($1s$ -, $2s$ -, $2p$ - like states) [64, 65]. In TMDs, excitons in K/K' valley resemble the physics of the 2D hydrogen, while the three-fold crystal field, band topology, the unusual 2D screening, and broken mirror symmetry lead to weak excitonic energy splitting and mixing [16, 22, 66–70]. In the X and Y valleys of the d -wave 2DAM, $E_{cv}(\mathbf{k})$ has a strong anisotropy, related by $\{T||C_{4z}\}$ rotation. This valley-dependent anisotropy originates from the inequivalent magnetic sublattices and is a key distinction between AM and their antiferromagnetic counterparts. Compared with the isotropic limit, H_{BSE} has a reduced symmetry due to the anisotropy in $E_{cv}(\mathbf{k})$, analogous to the effect of a crystal field on an impurity ion [71]. Excitons in phosphorene show how the anisotropy strongly influences excitonic properties [7, 72].

Both $\mathcal{D}_{\tau,\mathbf{k}}^\sigma$ and $\mathcal{A}_{\tau,\mathbf{k}}^S$ transform as irreducible representations (IRs) of the little group G_τ (denoted by $\Gamma_{\mathcal{D}^\sigma}$ and $\Gamma_{\mathcal{A}}$). From Eq. (1), $\mathcal{M}_{\tau,\sigma}^S$ transforms as the product

$$\Gamma_{\mathcal{D}^\sigma} \otimes \Gamma_{\mathcal{A}}^\dagger = (\Gamma_c^\dagger \otimes \Gamma_{\hat{v}_\sigma} \otimes \Gamma_v) \otimes \Gamma_{\mathcal{A}}^\dagger, \quad (3)$$

where $\Gamma_{c(v)}$ and $\Gamma_{\hat{v}_\sigma}$ are the IRs of conduction (valence) band and of light with σ polarization. The excitonic optical selection rules can be read from Eq. (3) as: An exciton is optically active under light with polarization σ , if $\Gamma_{\mathcal{D}^\sigma} \otimes \Gamma_{\mathcal{A}}^\dagger$ transform as the identity IR of the little group G_τ in valley τ . This establishes the excitonic optical selection rules through group representation theory.

The symmetry of AM is described by the SSG, which allows independent spin and real space operations, in the limit of negligible of SOC [47]. In our case, two spin-polarized X and Y valleys are connected by $\{T||C_{4z}\}$, the

TABLE I. Multiplication relations and basis functions of $\Gamma_i^{\mathbb{R}}$ of SSG ${}^12^1m^1m^\infty m1$.

	$\Gamma_1^{\mathbb{R}}$	$\Gamma_2^{\mathbb{R}}$	$\Gamma_3^{\mathbb{R}}$	$\Gamma_4^{\mathbb{R}}$	Functions
$\Gamma_1^{\mathbb{R}}$	$\Gamma_1^{\mathbb{R}}$	$\Gamma_2^{\mathbb{R}}$	$\Gamma_3^{\mathbb{R}}$	$\Gamma_4^{\mathbb{R}}$	$z, x^2 + y^2, x^2 - y^2, z^2$
$\Gamma_2^{\mathbb{R}}$		$\Gamma_1^{\mathbb{R}}$	$\Gamma_4^{\mathbb{R}}$	$\Gamma_3^{\mathbb{R}}$	R_z, xy
$\Gamma_3^{\mathbb{R}}$			$\Gamma_1^{\mathbb{R}}$	$\Gamma_2^{\mathbb{R}}$	x, xz
$\Gamma_4^{\mathbb{R}}$				$\Gamma_1^{\mathbb{R}}$	y, yz

little group G_τ is identical to that of a collinear ferromagnet. For this reason, $\mathcal{M}_{\tau,S}^\sigma$ in two valleys are also linked by $\{T||C_{4z}\}$: The excitonic optical response is valley-selective for linearly polarized light along x/y direction, but valley-indistinguishable for circular polarization. We focus on optical response of x/y polarized light $\mathcal{M}_{\tau,S}^{x/y}$ to take advantage of the valley degree of freedom. The relations $\mathcal{D}_{X,\mathbf{k}}^{x/y} = \mathcal{D}_{Y,\mathbf{k}}^{y/x}$ and $\mathcal{M}_{X,S}^{x/y} = \mathcal{M}_{Y,S'}^{y/x}$, with $|X, S\rangle$ and $|Y, S'\rangle$ form a pair of valley degenerate excitonic states, and their wave functions are protected by $\{T||C_{4z}\}$.

The IRs of G_τ form combinations of the real space and spin part: $\Gamma_i^{\mathbb{R}}\Gamma_j^{\mathbb{S}}$, where $\Gamma_i^{\mathbb{R}}$ denotes the i -th IR of the space group formed by the pure real space operations of G_τ ; $\Gamma_j^{\mathbb{S}}$ denotes the IR of its spin-only group, with $j = \uparrow / \downarrow$ denotes the spin $\pm 1/2$ IR and $j = 1$ denotes the identity IR. By separating the real and the spin space parts, $\mathcal{M}_{\tau,\sigma}^S$ transforms as $\Gamma_{\mathcal{D}^\sigma}^{\mathbb{R}}\Gamma_{\mathcal{D}^\sigma}^{\mathbb{S}} \otimes \Gamma_{\mathcal{A}}^{\mathbb{R}}\Gamma_{\mathcal{A}}^{\mathbb{S}\dagger} = (\Gamma_{\mathcal{D}^\sigma}^{\mathbb{R}} \otimes \Gamma_{\mathcal{A}}^{\mathbb{R}\dagger})(\Gamma_{\mathcal{D}^\sigma}^{\mathbb{S}} \otimes \Gamma_{\mathcal{A}}^{\mathbb{S}\dagger})$. The excitonic optical selection rules are now simplified to require $\mathcal{D}_{\tau,\mathbf{k}}^\sigma$ and $[\mathcal{A}_{\tau,\mathbf{k}}^S]^*$ transform as the same IR for both real and spin space parts.

We start from the spin space part. The selection rules require $\Gamma_{\mathcal{D}^\sigma}^{\mathbb{S}} \otimes \Gamma_{\mathcal{A}}^{\mathbb{S}\dagger} = (\Gamma_c^{\mathbb{S}\dagger} \otimes \Gamma_{\hat{v}_\sigma}^{\mathbb{S}} \otimes \Gamma_v^{\mathbb{S}}) \otimes \Gamma_{\mathcal{A}}^{\mathbb{S}\dagger} = \Gamma_1^{\mathbb{S}}$. Since both $\Gamma_{\hat{v}_\sigma}^{\mathbb{S}}$ and $\Gamma_{\mathcal{A}}^{\mathbb{S}}$ are identity IR of the spin-only group, the selection rules are simplified to $\Gamma_c^{\mathbb{S}\dagger} \otimes \Gamma_v^{\mathbb{S}} = \Gamma_1^{\mathbb{S}}$, which is equivariant to $\Gamma_c^{\mathbb{S}} = \Gamma_v^{\mathbb{S}} = \Gamma_{\uparrow/\downarrow}^{\mathbb{S}}$. In summary, we recover the spin selection rules that require bright excitons to be formed with electrons and holes with the same spin.

Next, we examine the real space part. This part varies in different d -wave 2DAM, allowing more complex and interesting selection rules, as compared to the spin space part. As an example, we choose $G_\tau = {}^12^1m^1m^\infty m1$, where the real space part is the point group $2mm$. The multiplication relations and basis functions of the real space IR $\Gamma_i^{\mathbb{R}}$ are summarized in Table I. We see from the table that s -, p_x -, p_y - and d_{xy} - excitons transform as $\Gamma_1^{\mathbb{R}}$, $\Gamma_3^{\mathbb{R}}$, $\Gamma_4^{\mathbb{R}}$, and $\Gamma_2^{\mathbb{R}}$, while $\hat{v}_{x/y}$ transforms as $\Gamma_3^{\mathbb{R}}/\Gamma_4^{\mathbb{R}}$. In the following, we study excitonic optical selection rules for C1 and C2 cases of the combination of orbital of conduction and valence bands characterized by $\Gamma_c^\dagger \otimes \Gamma_v$.

In C1, the real space part of $\Gamma_c^\dagger \otimes \Gamma_v$ is $\Gamma_3^{\mathbb{R}}$ or $\Gamma_4^{\mathbb{R}}$. As an example, we examine where $\Gamma_c^\dagger \otimes \Gamma_v$ transforms as $\Gamma_3^{\mathbb{R}}\Gamma_\uparrow^{\mathbb{S}}$ in the X valley, $\Gamma_4^{\mathbb{R}}\Gamma_\downarrow^{\mathbb{S}}$ in the Y valley. $\mathcal{D}_{X,\mathbf{k}}^{x/y}$ transforms as $\Gamma_1^{\mathbb{R}}\Gamma_\uparrow^{\mathbb{S}}/\Gamma_2^{\mathbb{R}}\Gamma_\uparrow^{\mathbb{S}}$, while $\mathcal{D}_{Y,\mathbf{k}}^{x/y}$ transforms as $\Gamma_2^{\mathbb{R}}\Gamma_\downarrow^{\mathbb{S}}/\Gamma_1^{\mathbb{R}}\Gamma_\downarrow^{\mathbb{S}}$.

We can see that both s - and d_{xy} -like excitons should be

TABLE II. The excitonic optical selection rules, with \checkmark for non-zero quantity. For the same type of Hamiltonian but different valleys, exciton energies are degenerate and non-zero excitonic optical transitions are equal [in the same cell of the table]. For example, $\Omega_X^{2p_y} = \Omega_Y^{2p_x}$ and $\mathcal{M}_{X,2p_y}^x = \mathcal{M}_{Y,2p_x}^y$.

σ		$\mathcal{M}_{X,1s}^\sigma$	$\mathcal{M}_{Y,1s}^\sigma$	$\mathcal{M}_{X,2p_y}^\sigma$	$\mathcal{M}_{Y,2p_x}^\sigma$	$\mathcal{M}_{X,2p_x}^\sigma$	$\mathcal{M}_{Y,2p_y}^\sigma$
Case 1 [Eq. (5)]	x	\checkmark	0	0	0	0	0
	y	0	\checkmark	0	0	0	0
Case 2 [Eq. (6)]	x	0	0	\checkmark	0	0	\checkmark
	y	0	0	0	\checkmark	\checkmark	0

bright as they transform as $\Gamma_1^{\mathbb{R}}$ and $\Gamma_2^{\mathbb{R}}$, but the brightness of a d -like exciton is much weaker than an s -like exciton, due to a much smaller wave amplitude. Therefore, the excitonic optical selection rules are simplified as s -like excitons in X/Y valley are coupled to x/y polarized light. This rule is reflected in Table II. One can verify that by exchanging the orbital characters of the X and Y valleys, the polarization and valley index coupling are exchanged.

In C2, the real space part of $\Gamma_c^\dagger \otimes \Gamma_v$ transforms as $\Gamma_1^{\mathbb{R}}$ or $\Gamma_2^{\mathbb{R}}$. As an example, we present the case where $\Gamma_c^\dagger \otimes \Gamma_v$ is $\Gamma_2^{\mathbb{R}}$ in both valleys. $\mathcal{D}_{\tau,\mathbf{k}}^{x/y}$ transforms as $\Gamma_4^{\mathbb{R}}/\Gamma_3^{\mathbb{R}}$ in both valleys. According to the excitonic optical selection rules, $2p_y$ - and $2p_x$ -like excitons are bright under x (y) polarized light, since their wave functions transform as $\Gamma_4^{\mathbb{R}}$ ($\Gamma_3^{\mathbb{R}}$). Together with the $\{T||C_{4z}\}$ transformation that links the exciton wave functions of a valley-degenerate exciton pair, $\mathcal{A}_{X,\mathbf{k}}^{2p_x/y}$ and $\mathcal{A}_{Y,\mathbf{k}}^{2p_y/x}$, we get an alternating optical selection rules of excitons. One example is that $2p_y$ -like exciton in the X valley and the $2p_x$ -like exciton in Y valley are optically active to x and y polarized light separately, with the same excitonic energy $\Omega_X^{2p_y} = \Omega_Y^{2p_x}$ and optical absorption strength $\mathcal{M}_{X,2p_y}^{x/y} = \mathcal{M}_{Y,2p_x}^{y/x}$. A summary is shown in Table II. So far, we have established the excitonic optical selection through symmetry analysis. We verify these predictions and get more insights by solving the BSE to obtain the measurable absorption of linearly-polarized light as a function of its frequency, ω

$$\alpha^{x/y}(\omega) = \frac{4e^2\pi^2}{c\omega} \sum_{S,\tau=X,Y} |\mathcal{M}_{\tau,S}^{x/y}|^2 \delta(\hbar\omega - \Omega_\tau^S), \quad (4)$$

where c is speed of light, δ is the delta function. The corresponding single-particle energies and states are obtained from the symmetry restricted effective Hamiltonian [73] for C1 in and C2 given below, with the selected parameters given in the Supplemental Material [57], to evaluate $\mathcal{M}_{\tau,S}^{x/y}$.

For C1, the low-energy effective Hamiltonian is

$$\begin{aligned} H_{X(\uparrow)}^1 &= (\Delta + \beta_1 k_x^2 + \beta_2 k_y^2) \sigma_z + \gamma k_x \sigma_y, \\ H_{Y(\downarrow)}^1 &= (\Delta + \beta_1 k_y^2 + \beta_2 k_x^2) \sigma_z + \gamma k_y \sigma_y, \end{aligned} \quad (5)$$

where, $k_{x,y}$ are the components of wave vectors measured from the band extremes at the X and Y points, σ denotes the Pauli matrices that act on a basis of conduction

and valence band edge states. An alternative realization of the C1 Hamiltonian is realized by the transformation $k_x \rightarrow k_y$ and $k_y \rightarrow -k_x$. The single-particle energy and state is obtained by solving $H_{\tau(\uparrow/\downarrow)}^1 |\tau, n\mathbf{k}\rangle = \epsilon_n |\tau, n\mathbf{k}\rangle$ with $n = v, c$ for the valence, conduction band. The velocity matrix elements can be obtained directly as $\mathcal{D}_{X,\mathbf{k}}^x = \mathcal{D}_{Y,\mathbf{k}}^y = \gamma$ and $\mathcal{D}_{X,\mathbf{k}}^y = \mathcal{D}_{Y,\mathbf{k}}^x = 0$. By solving the BSE in Eq. (2), we get the absorption spectrum as in Figs. 1(b) and (c). As shown in Figs. 1(d), (e), the corresponding exciton wave functions are s -like with alternating anisotropy in the two valleys. Our numerical results confirm that $1s$ -exciton in the X/Y valley is coupled to x/y polarized light as obtained from the group theory analysis. We also confirm that exciton wavefunctions $\mathcal{A}_{X,\mathbf{k}}^{1s}$ and $\mathcal{A}_{Y,\mathbf{k}}^{1s}$ are connected by $\{T||C_{4z}\}$, as predicted from our symmetry analysis.

For C2, the low-energy effective Hamiltonian is

$$\begin{aligned} H_{X(\uparrow)}^2 &= (\Delta + \beta_1 k_x^2 + \beta_2 k_y^2) \sigma_z + \gamma' k_x k_y \sigma_x, \\ H_{Y(\downarrow)}^2 &= (\Delta + \beta_1 k_y^2 + \beta_2 k_x^2) \sigma_z - \gamma' k_x k_y \sigma_x. \end{aligned} \quad (6)$$

An alternative C2 Hamiltonian is realized by replacing the second term by $(\gamma_1 k_x^2 + \gamma_2 k_y^2) \sigma_x$ or $(\gamma_1 k_y^2 + \gamma_2 k_x^2) \sigma_x$ for the X or Y valley Hamiltonian. The velocity matrix elements in the X and Y valleys are connected by $\{T||C_{4z}\}$, to satisfy $\mathcal{D}_{X,\mathbf{k}}^x = -\mathcal{D}_{Y,\mathbf{k}}^y = \gamma' k_y$ and $\mathcal{D}_{X,\mathbf{k}}^y = -\mathcal{D}_{Y,\mathbf{k}}^x = \gamma' k_x$ agreeing with numerically calculation in Figs. 2(d)-(g). In Figs. 2(b), (c), there are two peaks in the absorption spectra of x - and y -polarized light, with alternating coupling to X and Y valleys. Symmetries of excitons are identified by plotting their wave functions as shown in Figs. 2(h)-(k). Therefore, we find that the excitonic states $|X(Y), 2p_{y(x)}\rangle$ and $|Y(X), 2p_{y(x)}\rangle$ are responsible for the first and second peaks in the absorption of x (y) polarized light, respectively. The alternating excitonic optical selection rules are summarized in Table II. In Figs. 2(b), (c), the first peaks are higher than the second, indicating the relationship $\mathcal{M}_{X,2p_y}^x > \mathcal{M}_{X,2p_x}^y$. This is the result of the anisotropy of the exciton wave functions, such that $\mathcal{A}_{X,\mathbf{k}}^{2p_y}$ and $\mathcal{A}_{X,\mathbf{k}}^{2p_x}$ are stretched along their p -wave lobe direction and vertical direction, respectively [Figs. 2(h)-(k)]. As a result, the former is larger when multiplied by $\mathcal{D}_{X,\mathbf{k}}^{x/y}$, which disperses linearly in k . We expect a reduced/enhanced anisotropy of the band dispersion by adjusting β_x/β_y to make the heights of two

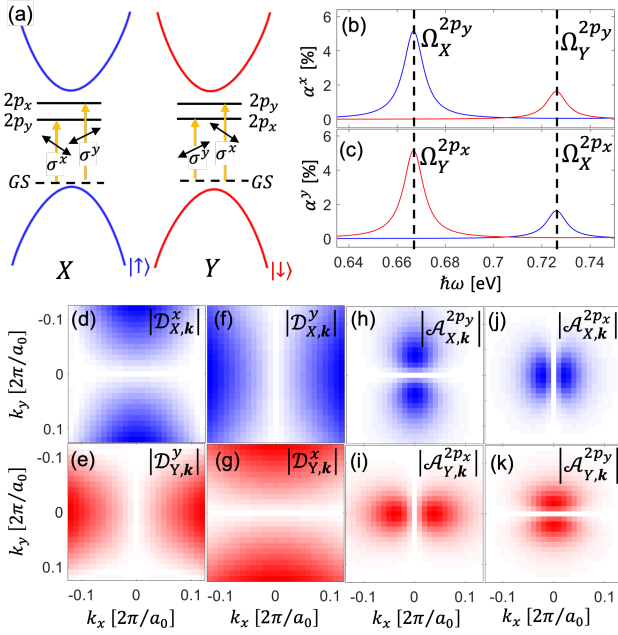


FIG. 2. Case 2, with the X (blue) and Y (red) valleys. (a) Schematic of the excitonic optical selection rules. (b), (c) Absorption spectra of x and y polarized light. (d)-(g) The velocity matrix elements $|\mathcal{D}_{\tau,k}^{x/y}|$. (h)-(k) The exciton wave function, with $2p_{y/x}$ -like exciton in the X/Y valley and $2p_{y/x}$ -like exciton in the Y/X valley corresponds to the x/y absorption of the first and second peak as in (b), (c).

peaks closer/further. This can be achieved by strain or electric field. The excitonic optical selection rules of both types are summarized in Table. II.

We next discuss how to lift the valley degeneracy of excitonic energies. In TMDs, an application of the magnetic field leads only to a small Zeeman splitting of ~ 0.1 - 0.2 meV/T [19], which can be enhanced up to 16 meV/T by proximity effect from magnetic substrate [19, 74]. Instead, another mechanism is particularly important for 2DAM: Strong piezomagnetism leads to a significant valley splitting upon the application of strain. An efficient valley splitting of 0.15 eV under 5% uniaxial strain for V_2Se_2O is obtained, as illustrated in Fig. 3(a) [39]. By calculating the evolution absorption spectra under strain based on C1 Hamiltonian in Eq. (5), we show that a redshift of y -polarized absorption is 0.15 eV larger than the energy shift for x polarized light, in Figs. 3(b), (c). This shift reflects the strain-induced difference of the exciton energies in the X and Y valleys. The obtained energy shifts originate mostly from the strain-induced change in the single-particle band edge energy: $\Delta\Omega^S = \Delta E_{cv}(\mathbf{k} = 0)$, with negligible role of strain-dependent changes in the exciton binding energy. The exciton-dominated absorption spectra evolution thus provides a fingerprint of the efficient lifting of the valley degeneracy, and guidance to strain engineering of optoelectronic devices.

The spin-valley locking in the d -wave 2DAM along with the valley-sensitive selection rules for the optical

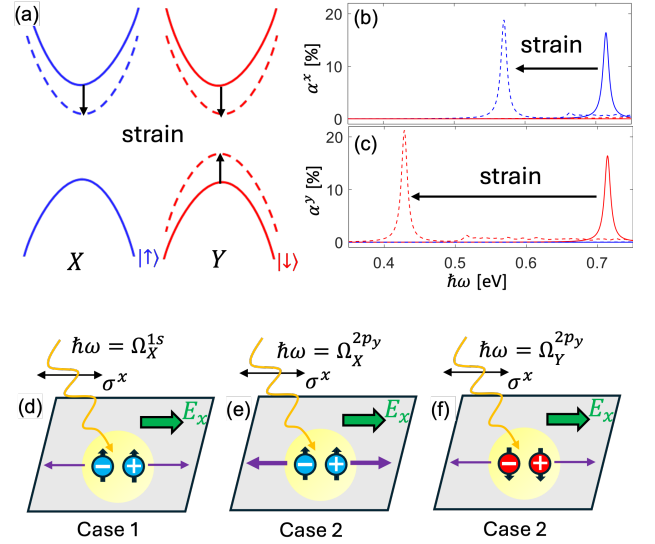


FIG. 3. (a) Schematic of the band edge motion under strain. (b), (c) Evolution of the absorption spectra under strain. Splitting of the peaks with different polarization reflects the broken valley degeneracy. (d)-(f) Anisotropic valley-polarized photocurrent with optical excitation and electric field.

absorption imply the realization of interesting valley-spin-polarized anisotropic photocurrents, illustrated in Figs. 3(d)-(f). With a photoexcitation of an appropriate frequency applied to the AM sample generates excitons which then disassociate to electrons and holes by the applied in-plane electric field with the formation of the electrical current. Let us consider the photocurrents for an applied electric field, E_x , along x . In C1, the light with angular frequency Ω_r^{1s}/\hbar and linear polarization along x generates excitons only in the X valley, with their subsequent conversion to the photocurrent $j_x = \sigma_{xx}^\tau E_x$, as shown in Fig. 3(d), where σ_{xx}^X is the photoconductivity in X valley along the x direction. Choosing the linear polarization along y will produce the photocurrent in the Y valley, now with a different magnitude of the current $j_x = \sigma_{xx}^Y E_x$, due to anisotropic band structure of AM ($\sigma_{xx}^X \neq \sigma_{xx}^Y$). In C2 AM, we can realize a similar situation without changing the linear polarization of the incident light, but by tuning the resonant excitation frequency instead. For the x polarization of light, we get the photocurrent, j_x^X , in the X valley for $\Omega_X^{2p_y}$ while taking different $\Omega_Y^{2p_y}$ will give us the photocurrent, j_x^Y , in the Y valley, as shown in Figs. 3(e)-(f). These photocurrents have different magnitudes, $j_x^X \neq j_x^Y$, due to the band structure anisotropy. The same notation is used in Figs. 1(b), (c) and Figs. 2(b), (c).

Following the theoretical prediction of V_2Te_2O and V_2Se_2O , there is rapid progress in the first-principles calculations and experiments that expand, study, and experimentally confirm the family of d -wave 2DAM with spin-polarized X/Y valleys, providing opportunities to test our predictions of exciton properties in real materials [39–43]. Among them, by breaking the out-of-plane mirror

symmetry of V_2Se_2O , e.g., by tailoring Janus monolayers, substrates, electric field, the valley properties can be described by the case 1 (Eq. (5) [57]). Our work in the case 2 [Eq. (6)] provides a guidance for material screening with alternating excitonic optical selection rules.

While SOC is not included in our theory, the large valley spin splitting from AM order makes spins robust against SOC, and justify its neglect. Even with our focus on the X/Y valley physics of d -wave 2DAM, the generic framework that relies on the fundamental group theory can also be generalized to g - and f - wave AM, while they do not have spin-polarized valleys and valley-selective light-valley coupling at high symmetry points.

Future studies of 2DAM may take advantage of this light-valley coupling as the tunability by uniaxial strain was also employed for ultrafast polarization switching and information transfer in spin-lasers [75]. With their complex spin textures, these 2DAM may also advance opportunities for an unconventional spin-orbit torque to integrate spintronics, electronics, and photonics [76].

This work is supported by the U.S. Department of Energy, Office of Science, Basic Energy Sciences under Award No. DE-SC0004890. Computational resources were provided by the UB Center for Computational Research.

-
- [1] Y. Zhang, Y.-W. Tan, H. L. Stormer, and P. Kim, Experimental observation of the quantum Hall effect and Berry's phase in graphene, *Nature* **438**, 201 (2005).
- [2] K. S. Burch, D. Mandrus, and J.-G. Park, Magnetism in two-dimensional van der Waals materials, *Nature* **563**, 47 (2018).
- [3] M. N. Brunetti, O. L. Berman, and R. Y. Kezerashvili, Optical properties of anisotropic excitons in phosphorene, *Phys. Rev. B* **100**, 155433 (2019).
- [4] D. Huang, J. Choi, C. Shih, and X. Li, Excitons in semiconductor Moiré superlattices, *Nat. Nanotechnol.* **17**, 227 (2022).
- [5] M. Grzeszczyk, S. Acharya, D. Pashov, Z. Chen, K. Vakinova, M. van Schilfgaarde, K. Watanabe, T. Taniguchi, K. S. Novoselov, M. I. Katsnelson, and M. Koperski, Strongly correlated exciton-magnetization system for optical spin pumping in $CrBr_3$ and CrI_3 , *Adv. Mater.* **35**, 2209513 (2023).
- [6] X. Wang, A. M. Jones, K. L. Seyler, V. Tran, Y. Jia, H. Zhao, H. Wang, L. Yang, X. Xu, and F. Xia, Highly anisotropic and robust excitons in monolayer black phosphorus, *Nat. Nanotechnol.* **10**, 517 (2015).
- [7] V. Tran, R. Soklaski, Y. Liang, and L. Yang, Layer-controlled band gap and anisotropic excitons in few-layer black phosphorus, *Phys. Rev. B* **89**, 235319 (2014).
- [8] D. Van Tuan, B. Scharf, Z. Wang, J. Shan, K. F. Mak, I. Žutić, and H. Dery, Probing many-body interactions in monolayer transition-metal dichalcogenides, *Phys. Rev. B* **99**, 085301 (2019).
- [9] Y. Shao, F. Dirnberger, S. Qiu, S. Acharya, S. Terres, E. J. Telford, D. Pashov, B. S. Y. Kim, F. L. Ruta, D. G. Chica, A. H. Dismukes, M. E. Ziebel, Y. Wang, J. Choe, Y. J. Bae, A. J. Millis, M. I. Katsnelson, K. Mosina, Z. Sofer, R. Huber, X. Zhu, X. Roy, M. van Schilfgaarde, A. Chernikov, and D. N. Basov, Magnetically confined surface and bulk excitons in a layered antiferromagnet, *Nat. Mater.* **354**, aag1992 (2025).
- [10] G. Wang, A. Chernikov, M. M. Glazov, T. F. Heinz, X. Marie, T. Amand, and B. Urbaszek, Colloquium: Excitons in atomically thin transition metal dichalcogenides, *Rev. Mod. Phys.* **90**, 021001 (2018).
- [11] D. Unuchek, A. Ciarrocchi, K. Watanabe, T. Taniguchi, and A. Kis, Room-temperature electrical control of exciton flux in a van der Waals heterostructure, *Nature* **560**, 340 (2018).
- [12] Z. Zhou, E. A. Szwed, D. J. Choksy, L. H. Fowler-Gerace, and L. V. Butov, Long-distance decay-less spin transport in indirect excitons in a van der Waals heterostructure, *Nat. Commun.* **15**, 9454 (2024).
- [13] P. Y. Yu and M. Cardona, *Fundamentals of Semiconductors: Physics and Materials Properties, 4th Edition* (Springer, Berlin, 2010).
- [14] D. Xiao, G.-B. Liu, W. Feng, X. Xu, and W. Yao, Coupled spin and valley physics in monolayers of MoS_2 and other group-VI dichalcogenides, *Phys. Rev. Lett.* **108**, 196802 (2012).
- [15] Q. Wang, K. Kalantar-Zadeh, A. Kis, J. N. Coleman, and M. S. Strano, Electronics and optoelectronics of two-dimensional transition metal dichalcogenides, *Nat. Nanotechnol.* **7**, 699 (2012).
- [16] A. Chernikov, T. C. Berkelbach, H. M. Hill, A. Rigosi, Y. Li, B. Aslan, D. R. Reichman, M. S. Hybertsen, and T. F. Heinz, Exciton binding energy and nonhydrogenic Rydberg series in monolayer WS_2 , *Phys. Rev. Lett.* **113**, 076802 (2014).
- [17] X. Chen, Z. Lian, Y. Meng, L. Ma, and S.-F. Shi, Excitonic complexes in two-dimensional transition metal dichalcogenides, *Nat. Commun.* **14** (2023).
- [18] X. Xu, W. Yao, and T. F. Heinz, Spin and pseudospins in layer transition metal dichalcogenides, *Nat. Phys.* **10**, 343 (2014).
- [19] I. Žutić, A. Matos-Abiague, B. Scharf, H. Dery, and K. Belashchenko, Proximitized materials, *Mater. Today* **22**, 85 (2019).
- [20] B. Scharf, G. Xu, A. Matos-Abiague, and I. Žutić, Magnetic proximity effects in transition-metal dichalcogenides: Converting excitons, *Phys. Rev. Lett.* **119**, 127403 (2017).
- [21] C. Serati de Brito, P. E. Faria Junior, T. S. Ghiasi, J. Ingla-Aynés, C. R. Rabahi, C. Cavalini, F. Dirnberger, S. Mañas-Valero, K. Watanabe, T. Taniguchi, K. Zollner, J. Fabian, C. Schüller, H. S. J. van der Zant, and Y. G. Gobato, Charge transfer and asymmetric coupling of $MoSe_2$ valleys to the magnetic order of $CrSBr$, *Nano Lett.* **23**, 11073 (2023).
- [22] J. D. Cao, G. Xu, B. Scharf, K. Denisov, and I. Žutić, Emergent bright excitons with Rashba spin-orbit coupling in atomic monolayers, *Phys. Rev. B* **109**, 085407 (2024).
- [23] P. E. Faria Junior and J. Fabian, Signatures of elec-

- tric field and layer separation effects on the spin-valley physics of MoSe₂/WSe₂ heterobilayers: From energy bands to dipolar excitons, *Nanomaterials* **13**, 1187 (2023).
- [24] F. Wu, T. Lovorn, and A. H. MacDonald, Topological exciton bands in Moiré heterojunctions, *Phys. Rev. Lett.* **118**, 147401 (2017).
- [25] L. Šmejkal, J. Sinova, and T. Jungwirth, Beyond conventional ferromagnetism and antiferromagnetism: A phase with nonrelativistic spin and crystal rotation symmetry, *Phys. Rev. X* **12**, 031042 (2022).
- [26] I. Mazin, Editorial: Altermagnetism—A new punch line of fundamental magnetism, *Phys. Rev. X* **12**, 040002 (2022).
- [27] H. Bai, L. Han, X. Y. Feng, Y. J. Zhou, R. X. Su, Q. Wang, L. Y. Liao, W. X. Zhu, X. Z. Chen, F. Pan, X. L. Fan, and C. Song, Observation of spin splitting torque in a collinear antiferromagnet, *Phys. Rev. Lett.* **128**, 197202 (2022).
- [28] J. Krempaský, L. Šmejkal, S. D'souza, M. Hajlaoui, G. Springholz, K. Uhlířová, F. Alarab, P. Constantinou, V. Strocov, D. Usanov, *et al.*, Altermagnetic lifting of Kramers spin degeneracy, *Nature* **626**, 517 (2024).
- [29] C. Song, H. Bai, Z. Zhou, L. Han, H. Reichlova, J. H. Dil, J. Liu, X. Chen, and F. Pan, Altermagnets as a new class of functional materials, *Nat. Rev. Mater.* , 473 (2025).
- [30] K. D. Belashchenko, Giant strain-induced spin splitting effect in MnTe, a *g*-wave altermagnetic semiconductor, *Phys. Rev. Lett.* **134**, 086701 (2025).
- [31] K. S. Denisov and I. Žutić, Anisotropic spin dynamics in antiferromagnets with a nonrelativistic spin splitting, *Phys. Rev. B* **110**, L180403 (2024).
- [32] I. Khan, D. Bezzerga, B. Marfoua, and J. Hong, Altermagnetism, piezovolley, and ferroelectricity in two-dimensional Cr₂SeO altermagnet, *npj 2D Mater. Appl.* **9**, 18 (2025).
- [33] S. Hayami, Y. Yanagi, and H. Kusunose, Momentum-dependent spin splitting by collinear antiferromagnetic ordering, *J. Phys. Soc. Jpn.* **88**, 123702 (2019).
- [34] S. Hayami, Y. Yanagi, and H. Kusunose, Spontaneous antisymmetric spin splitting in noncollinear antiferromagnets without spin-orbit coupling, *Phys. Rev. B* **101**, 220403 (2020).
- [35] I. I. Mazin, K. Koepernik, M. D. Johannes, R. González-Hernández, and L. Šmejkal, Prediction of unconventional magnetism in doped FeSb₂, *Proc. Natl. Acad. Sci. U.S.A.* **118**, e2108924118 (2021).
- [36] L.-D. Yuan, Z. Wang, J.-W. Luo, E. I. Rashba, and A. Zunger, Giant momentum-dependent spin splitting in centrosymmetric low-*z* antiferromagnets, *Phys. Rev. B* **102**, 014422 (2020).
- [37] X. Duan, J. Zhang, Z. Zhu, Y. Liu, Z. Zhang, I. Žutić, and T. Zhou, Antiferroelectric altermagnets: Antiferroelectricity alters magnets, *Phys. Rev. Lett.* **134**, 106801 (2025).
- [38] M. Gu, Y. Liu, H. Zhu, K. Yananose, X. Chen, Y. Hu, A. Stroppa, and Q. Liu, Ferroelectric switchable altermagnetism, *Phys. Rev. Lett.* **134**, 106802 (2025).
- [39] H.-Y. Ma, M. Hu, N. Li, J. Liu, W. Yao, J.-F. Jia, and J. Liu, Multifunctional antiferromagnetic materials with giant piezomagnetism and noncollinear spin current, *Nat. Commun.* **12**, 2846 (2021).
- [40] B. Jiang, M. Hu, J. Bai, Z. Song, C. Mu, G. Qu, W. Li, W. Zhu, H. Pi, Z. Wei, Y.-J. Sun, Y. Huang, X. Zheng, Y. Peng, L. He, S. Li, J. Luo, Z. Li, G. Chen, H. Li, H. Weng, and T. Qian, A metallic room-temperature d-wave altermagnet, *Nat. Phys.* **21**, 754 (2025).
- [41] F. Zhang, X. Cheng, Z. Yin, C. Liu, L. Deng, Y. Qiao, Z. Shi, S. Zhang, J. Lin, Z. Liu, M. Ye, Y. Huang, X. Meng, C. Zhang, T. Okuda, K. Shimada, S. Cui, Y. Zhao, G.-H. Cao, S. Qiao, J. Liu, and C. Chen, Crystal-symmetry-paired spin–valley locking in a layered room-temperature metallic altermagnet candidate, *Nat. Phys.* **21**, 760 (2025).
- [42] R. Xu, Y. Gao, and J. Liu, Chemical design of monolayer altermagnets, *arXiv preprint arXiv:2505.15484* (2025), preprint.
- [43] Z. Zhu, X. Duan, J. Zhang, B. Hao, I. Žutić, and T. Zhou, Two-dimensional ferroelectric altermagnets: From model to material realization, *Nano Lett.* **x**, xxxx (2025).
- [44] W. F. Brinkman and R. J. Elliott, Theory of spin-space groups, *Proc. R. Soc. A* **294**, 343 (1966).
- [45] D. Litvin and W. Opechowski, Spin groups, *Physica* **76**, 538 (1974).
- [46] P. Liu, J. Li, J. Han, X. Wan, and Q. Liu, Spin-group symmetry in magnetic materials with negligible spin-orbit coupling, *Phys. Rev. X* **12**, 021016 (2022).
- [47] X. Chen, J. Ren, Y. Zhu, Y. Yu, A. Zhang, P. Liu, J. Li, Y. Liu, C. Li, and Q. Liu, Enumeration and representation theory of spin space groups, *Phys. Rev. X* **14**, 031038 (2024).
- [48] Z. Xiao, J. Zhao, Y. Li, R. Shindou, and Z.-D. Song, Spin space groups: Full classification and applications, *Phys. Rev. X* **14**, 031037 (2024).
- [49] Y. Jiang, Z. Song, T. Zhu, Z. Fang, H. Weng, Z.-X. Liu, J. Yang, and C. Fang, Enumeration of spin-space groups: Toward a complete description of symmetries of magnetic orders, *Phys. Rev. X* **14**, 031039 (2024).
- [50] J. Yang, Z.-X. Liu, and C. Fang, Symmetry invariants and classes of quasiparticles in magnetically ordered systems having weak spin-orbit coupling, *Nat. Commun.* **15**, 10203 (2024).
- [51] X. Chen, Y. Liu, P. Liu, Y. Yu, J. Ren, J. Li, A. Zhang, and Q. Liu, Unconventional magnons in collinear magnets dictated by spin space groups, *Nature* **640**, 349 (2025).
- [52] D.-F. Shao, S.-H. Zhang, G. Gurung, W. Yang, and E. Y. Tsymlal, Nonlinear anomalous Hall effect for Néel vector detection, *Phys. Rev. Lett.* **124**, 067203 (2020).
- [53] Y. Liu, J. Li, and Q. Liu, Chern-insulator phase in antiferromagnets, *Nano Lett.* **23**, 8650 (2023).
- [54] Y.-P. Zhu, X. Chen, X.-R. Liu, Y. Liu, P. Liu, H. Zha, G. Qu, C. Hong, J. Li, Z. Jiang, *et al.*, Observation of plaid-like spin splitting in a noncoplanar antiferromagnet, *Nature* **626**, 523 (2024).
- [55] Q. Liu, X. Dai, and S. Blügel, Different facets of unconventional magnetism, *Nat. Phys.* **626**, 523 (2025).
- [56] H. Zhu, J. Li, X. Chen, Y. Yu, and Q. Liu, Magnetic geometry induced quantum geometry and nonlinear transports, *Nat. Commun.* **16**, 1 (2025).
- [57] See Supplemental Material for a discussion on first-principles calculations, effective Hamiltonians, and computational details on the BSE.
- [58] F. Bechstedt, *Many-Body Approach to Electronic Excitations* (Springer, 2016).
- [59] M. Rohlfing and S. G. Louie, Electron-hole excitations and optical spectra from first principles, *Phys. Rev. B* **62**, 4927 (2000).

- [60] B. Scharf, T. Frank, M. Gmitra, J. Fabian, I. Žutić, and V. Perebeinos, Excitonic stark effect in MoS₂ monolayers, *Phys. Rev. B* **94**, 245434 (2016).
- [61] B. Scharf, D. V. Tuan, and I. Žutić, Dynamical screening in monolayer transition-metal dichalcogenides and its manifestations in the exciton spectrum, *J. Phys.: Cond. Matt.* **31**, 203001 (2019).
- [62] L. V. Keldysh, Coulomb interaction in thin semiconductor and semimetal films, *JETP Lett.* **29**, 658 (1979).
- [63] P. Cudazzo, I. V. Tokatly, and A. Rubio, Dielectric screening in two-dimensional insulators: Implications for excitonic and impurity states in graphane, *Phys. Rev. B* **84**, 085406 (2011).
- [64] X. L. Yang, S. H. Guo, F. T. Chan, K. W. Wong, and W. Y. Ching, Analytic solution of a two-dimensional hydrogen atom. I. Nonrelativistic theory, *Phys. Rev. A* **43**, 1186 (1991).
- [65] C. Y.-P. Chao and S. L. Chuang, Analytical and numerical solutions for a two-dimensional exciton in momentum space, *Phys. Rev. B* **43**, 6530 (1991).
- [66] M. M. Glazov, L. E. Golub, G. Wang, X. Marie, T. Amand, and B. Urbaszek, Intrinsic exciton-state mixing and nonlinear optical properties in transition metal dichalcogenide monolayers, *Phys. Rev. B* **95**, 035311 (2017).
- [67] P. Gong, H. Yu, Y. Wang, and W. Yao, Optical selection rules for excitonic Rydberg series in the massive Dirac cones of hexagonal two-dimensional materials, *Phys. Rev. B* **95**, 125420 (2017).
- [68] G. Xu, T. Zhou, B. Scharf, and I. Žutić, Optically probing tunable band topology in atomic monolayers, *Phys. Rev. Lett.* **125**, 157402 (2020).
- [69] A. Kormányos, V. Zólyomi, N. D. Drummond, P. Rakytá, G. Burkard, and V. I. Fal'ko, Monolayer MoS₂: Trigonal warping, the Γ valley, and spin-orbit coupling effects, *Phys. Rev. B* **88**, 045416 (2013).
- [70] X. Zhang, W.-Y. Shan, and D. Xiao, Optical selection rule of excitons in gapped chiral fermion systems, *Phys. Rev. Lett.* **120**, 077401 (2018).
- [71] M. S. Dresselhaus, G. Dresselhaus, and A. Jorio, *Group theory: Application to the physics of condensed matter* (Springer Science, 2007).
- [72] A. S. Rodin, A. Carvalho, and A. H. Castro Neto, Excitons in anisotropic two-dimensional semiconducting crystals, *Phys. Rev. B* **90**, 075429 (2014).
- [73] Y. Liu, J. Li, P. Liu, and Q. Liu, Unconventional spin textures emerging from a universal symmetry theory of spin-momentum locking, *npj Quantum Mater.* **9**, 69 (2024).
- [74] T. Norden, C. Zhao, P. Zhang, R. Sabirianov, A. Petrou, and H. Zeng, Giant valley splitting in monolayer WS₂ by magnetic proximity effect, *Nat. Commun.* **10**, 4163 (2019).
- [75] M. Lindemann, G. Xu, T. Pusch, R. Michalzik, M. R. Hofmann, I. Žutić, and N. C. Gerhardt, Ultrafast spin-lasers, *Nature* **568**, 212 (2019).
- [76] P. A. Dainone, N. F. Prestes, P. Renucci, A. Bouché, M. Morassi, X. Devaux, M. Lindemann, J.-M. George, H. Jaffrès, A. Lemaitre, X. B., M. Stoffel, T. Chen, L. Lombez, D. Lagarde, G. Cong, T. Ma, P. Pigeat, M. Vergnat, H. Rinnert, X. Marie, X. Han, S. Mangin, J.-C. Rojas-Sánchez, J.-P. Wang, N. C. Beard, I. Žutić, and Y. Lu, Controlling the helicity of light by electrical magnetization switching, *Nature* **627**, 783 (2024).